AGU PUBLICATIONS

JGR

Journal of Geophysical Research: Atmospheres

RESEARCH ARTICLE
10.1002/2014JD022924

Key Points:
- The MJO modulates the summer air temperature in Patagonia
- The amplitude of the intraseasonal air temperature modulation is ~1.5 K
- MJO phase 8 induces warm conditions and can favor the occurrence of heat waves

Supporting Information:
- Figures S1–S7

Correspondence to:
M. Jacques-Coper,
jacques@giub.unibe.ch

Citation:
Jacques-Coper, M., S. Brönnimann, O. Martius, C. S. Vera, and S. B. Cerne (2015), Evidence for a modulation of the intraseasonal summer temperature in Eastern Patagonia by the Madden-Julian Oscillation, *J. Geophys. Res. Atmos.*, *120*, doi:10.1002/2014JD022924.

Received 28 NOV 2014
Accepted 5 JUN 2015
Accepted article online 8 JUN 2015

Evidence for a modulation of the intraseasonal summer temperature in Eastern Patagonia by the Madden-Julian Oscillation

Martín Jacques-Coper[1], Stefan Brönnimann[1], Olivia Martius[1], Carolina S. Vera[2], and S. Bibiana Cerne[2]

[1]Oeschger Center for Climate Change Research and Institute of Geography, University of Bern, Bern, Switzerland, [2]Centro de Investigaciones del Mar y la Atmósfera, CIMA/CONICET-UBA, DCAO/FCEN, UMI-IFAECI/CNRS, Buenos Aires, Argentina

Abstract We describe the relationship between the intraseasonal component of surface air temperature (SAT) variability in Eastern Patagonia and the Madden-Julian Oscillation (MJO) during austral summer based on ~50 years of daily instrumental records, the Twentieth Century Reanalysis, and a century-long MJO index reconstruction. Our results show that the summer SAT variability in Patagonia is highly driven by the intraseasonal activity (~80%), especially by that associated with the MJO. The active MJO phases modulate the spatial mean intraseasonal temperature signal in Eastern Patagonia with ~1.5°C of amplitude. In most of the region, the warmest (coldest) conditions are found during active phase 8 (4). These opposite states of the temperature perturbations are related to almost inverse midlevel circulation anomalies over southern South America and the southwest Atlantic, which are part of a large-scale Rossby-like wave train of alternating circulation anomalies extended along the South Pacific. The corresponding outgoing longwave radiation anomalies suggest that these structures may be triggered by anomalous convection in the tropics. Furthermore, we show that intraseasonal heat waves in southeastern Patagonia tend to occur during active MJO phase 8. These events are also induced by a wave train pattern over the South Pacific, associated with other intraseasonal variability sources. Hence, as shown in a case study, circulation anomalies over the South Pacific triggered, in general, by tropical convection variability and, in particular, by the MJO activity may constructively interact with circulation patterns resulting from the extratropical dynamics, eventually leading to intraseasonal heat waves in southeastern Patagonia.

1. Introduction

Eastern Patagonia is the region of southern South America located south of 40°S and to the East of the Andes cordillera. At the western side of this mountain range, the forced ascent of the westerlies that blow from the Pacific leads to orographic rain; in contrast, the lee side is characterized by extremely windy conditions and high aridity, a phenomenon known as rain shadow effect. However, the temperature regimes in Patagonia are not strongly divided by the Andes [*Coronato and Bisigato*, 1998]. Eastern Patagonia exhibits a marked annual temperature cycle, which is a characteristic of a rather continental climate [*Garreaud et al*., 2012].

Climate variability on diverse time scales, in particular, that of temperature, can affect both natural and socioecological aspects in Patagonia. Despite its relatively low population density, desertification is an issue in Eastern Patagonia [*Del Valle et al*., 1998; *Mazzonia and Vazquez*, 2009]. In Western Patagonia, the Northern and Southern Patagonian Ice Fields comprise several glaciers, which constitute major fresh water reservoirs. In a long-term sense, these ice masses have retreated during the last decades [*Rasmussen et al*., 2007]. However, more research concerning the links between glaciers and climate is necessary, especially in this part of the world [*Dussaillant et al*., 2010; *Kargel et al*., 2012; *Willis et al*., 2012]. Thus, scientific efforts should focus on the various causes and effects of extended regional warm periods within different frequency bands.

During austral summer (December to February (DJF)), the continental heating is higher in the northern part of Eastern Patagonia than in the more austral zones, a fact that causes a meridional temperature gradient and hence a north-south pattern of temperature variability [*Prohaska*, 1976]. *Berman et al*. [2013] studied the year-to-year seasonal variability of surface air temperature (SAT) in this part of the world for 1979–2009 based on instrumental records and reanalysis. The authors divided Eastern Patagonia into a northern region and a southern region (~40°S–44°S and ~50°S–56°S, respectively). These regions showed

different summer temperature patterns within the analyzed period. For the northern part, the authors found that anticyclonic (cyclonic) anomalies extending over southern South America and cyclonic (anticyclonic) anomalies further to the south are associated with warm (cold) conditions in summer [*Berman et al*., 2013]. For the southern part of Eastern Patagonia, that study also showed that anticyclonic (cyclonic) anomalies centered over the southern tip of the continent and the adjacent oceans result in increased (reduced) incoming solar radiation during summer, thus contributing to local warm (cold) conditions. Furthermore, within a continental scale, *Berman et al*. [2013] found that SAT anomalies from southern Patagonia are negatively correlated with those over the central-southern region of Brazil, more than 3000 km to the north, thus defining a temperature dipole between the southern tip and subtropical areas of South America.

With a broader spatial and temporal perspective, *Jacques-Coper and Brönnimann* [2014] described the summer variability of SAT in Eastern Patagonia at interdecadal and interannual scales during the twentieth century. The main interannual mode exhibits a period of ~3.4 years and is associated with a wave train circulation pattern over the South Pacific, with alternating action centers in New Zealand, to the north of the Ross Sea, to the west of South America, and over Southern South America. This pattern, which resembles the Pacific-South American mode 2 [*Mo and Paegle*, 2001], presumably originates (at least partially) in the tropical West Pacific, and its circulation anomalies induce a teleconnection between the climates of Oceania and Eastern Patagonia.

Further own work [*Jacques-Coper et al*., 2015] has been devoted to understanding the role played by the intraseasonal variability on modulating strong and persistent warm conditions in southeastern Patagonia (SEPG, 46°S–52°S, 65°W–70°W), a subregion of Eastern Patagonia. These events, identified as local heat waves, exhibit a mean temperature anomaly larger than 4°C and typically last for ~2 weeks. That study found that the large-scale circulation pattern that triggers these intraseasonal heat waves resembles the wave train found for the seasonal scale in summer. Moreover, that work also addressed the temporal development of that large-scale circulation pattern, which gives rise to the teleconnection between Eastern Patagonia and Oceania and of the SAT perturbation within southern South America. In addition, the temperature dipole pattern between Eastern Patagonia and subtropical regions of the continent, which was observed for the seasonal means, was also found for the intraseasonal temperature anomalies. Notwithstanding, the source of the wave train-like atmospheric pattern leading to warm conditions in Eastern Patagonia remained an open aspect to explore in that work. Therefore, the possible tropical modulation of the intraseasonal SAT in Eastern Patagonia by the Madden-Julian Oscillation (MJO) [*Madden and Julian*, 1971] and the incidence of this mode in the occurrence of heat waves there are two of the main points addressed in the present study.

The intraseasonal variability range has been reported to exhibit a notorious impact in temperature (especially in minimum temperature) in southeastern South America during winter [*Naumann and Vargas*, 2012]. For this region and season, *Naumann and Vargas* [2010] showed consistent covariability of temperature and precipitation with the MJO. The MJO is the dominant mode of intraseasonal variability of the tropical coupled ocean-atmosphere system. It consists of a planetary-scale eastward propagating pattern of atmospheric circulation and deep convection, associated with anomalies in various variables in both tropical and subtropical regions [*Zhang*, 2005]. The modulation of regional weather and climate systems by the MJO, especially in subtropical latitudes, has been extensively studied, regarding both precipitation [e.g., *Sperber*, 2003; *Donald et al*., 2006; *Kanamori et al*., 2013; *Matthews et al*., 2013] and temperature [e.g., *Maloney and Kiehl*, 2002; *Oliver*, 2014; *Salby and Hendon*, 1994; *Zhou et al*., 2011]. Large-scale impacts associated with this mode have also been described for climates of higher latitudes, both in the Northern Hemisphere [*Vecchi and Bond*, 2004; *Cassou*, 2008] and in the Southern Hemisphere, in particular, South America [e.g., *Moore et al*., 2010; *Naumann and Vargas*, 2010; *Barrett et al*., 2011; *Juliá et al*., 2012].

Recently, *Alvarez et al*. [2015] described the seasonal variations of the MJO influence on both rainfall and surface temperature anomalies in South America based solely on reanalysis and restricted to 1979–2012. In particular, that study shows a significant MJO signal on positive (negative) temperature anomalies in southern South America during MJO phases 7–8 (3–4) during summer. However, that study did not provide a quantification of the modulation by the MJO of the summer SAT in Patagonia nor related the

Table 1. Stations From the Argentinean National Weather Service Used in This Study

Station Code	Station Name	Latitude	Longitude	Altitude (m asl)	Period Covered	T_x: Data Availability [%]	T_n: Data Availability (%)	Active MJO Phase With Lowest T_m	Active MJO Phase With Highest T_m
87715	Neuquén Aero	−38°57′	−68°08′	271	1957–2010	95.9	97.8	4	8
87736	Río Colorado	−39°01′	−64°05′	79	1957–2010	74.2	77.9	4	8
87750	Bahía Blanca Aero	−38°44′	−62°10′	83	1957–2010	99.1	99.1	5	7
87765	Bariloche Aero	−41°09′	−71°10′	840	1957–2010	95.2	99.4	4	8
87774	Maquinchao	−41°15′	−68°44′	888	1957–2010	94.4	95.8	4	8
87791	Viedma Aero	−40°51′	−63°01′	7	1968–2010	95.9	96.0	4	2
87803	Esquel Aero	−42°56′	−71°09′	797	1962–2010	91.0	91.7	3	8
87814	Paso de Indios	−43°49′	−68°53′	460	1969–2010	84.9	85.7	4	8
87828	Trelew Aero	−43°12′	−65°16′	43	1957–2010	99.8	99.8	4	8
87860	Comodoro Rivadavia Aero	−45°47′	−67°30′	46	1957–2010	98.5	98.5	4	8
87880	Gobernador Gregores Aero	−48°47′	−70°10′	358	1957–2010	62.8	70.6	4	8
87896	Puerto Deseado Aero	−47°44′	−65°55′	80	1957–2010	78.6	82.1	4	8
87903	Lago Argentino Aero	−50°20′	−72°18′	220	1957–2010	75.1	75.0	4	8
87909	San Julián Aero	−49°19′	−67°47′	62	1937–2010	61.8	65.3	4	8
87925	Río Gallegos Aero	−51°37′	−69°17′	19	1957–2010	94.4	96.8	4	8
87934	Río Grande B.A.	−53°48′	−67°45′	22	1960–2010	86.0	82.1	4	8

MJO to temperature extreme events such as heat waves there. Besides, no case studies on this subject in the literature could be found. All these aspects are key motivations for the present work.

Hence, to the best knowledge of the authors, no previous study has explicitly analyzed the relationship between intraseasonal temperature in Eastern Patagonia and the MJO during summer, with a long-term perspective on the twentieth century. Therefore, this subject is the original contribution of the present paper, with emphasis on the possible role played by the MJO in the triggering of intraseasonal heat waves in this region. A special novelty of this paper is that it comprises the analysis of long daily instrumental records, together with the Twentieth Century Reanalysis (20CR) and a century long reconstruction of the MJO. The said observational time series have not been assimilated in the reanalysis used here and thus constitute an independent data set to perform our research and compare our results. Due to its temporal coverage, the 20CR provides the possibility of exploring robust signals associated with a large number of extreme events, such as heat waves, in this case. The present work is structured as follows: section 2 introduces the data and methods used in this work, section 3.1 explains the decomposition of the SAT field to obtain the intraseasonal variability range of this variable, the modulation of intraseasonal summer SAT in Eastern Patagonia by the MJO is presented in section 3.2, section 3.3 shows the large-scale fields associated with the active phases of the MJO that lead to the greatest SAT departures in Eastern Patagonia, section 3.4 describes the connection found between intraseasonal heat waves in SEPG and the MJO, a case study illustrating the previous results is offered in section 3.5, and finally, section 4 discusses and summarizes our findings.

2. Data and Methods

2.1. Instrumental and Reanalysis Data

In this study we focus on austral summer, i.e., DJF (1 December to 28 February; seasons are assigned to the corresponding JF year). Nondetrended daily fields of the reanalysis ensemble means of SAT at 2 m and geopotential height at 500 hPa (z500) were accessed from the Twentieth Century Reanalysis version 2 (20CR) for DJF 1872–2010 [*Compo et al.*, 2011]. The interpolated outgoing longwave radiation (OLR) data set accessed from the National Center for Atmospheric Research spans DJF 1975–2013 with daily resolution and is available on a 2.5° × 2.5° global grid [*Liebmann and Smith*, 1996]. The observational temperature data sets used in this study were supplied by the Argentinean National Weather Service and contain information on minimum temperature (T_n) and maximum temperature (T_x) recorded by 16 stations (in most cases for DJF 1957–2010; see Table 1). The mean instrumental SAT (T_m) was calculated as the average of T_x and T_n.

With the aim of facilitating the intercomparison of results, the intraseasonal anomalies of each variable are defined in this paper after *Cerne and Vera* [2011], as the result of subtracting from the daily values their

corresponding climatological daily means (a term which accounts for the annual cycle) and the seasonal departures of each particular year from the climatology (i.e., the DJF mean of each year minus the long-term seasonal mean). That is, the intraseasonal anomaly of a given variable for day d and year y is calculated as

$$\begin{aligned}\text{intraseasonal anomaly}_{d,y} &= \text{daily value}_{d,y} - \text{climatological daily mean}_{d} \\ &- \left(\text{DJF seasonal mean}_{y} - \text{long–term DJF seasonal mean}\right)\end{aligned} \quad (1)$$

The reference period for defining long-term statistics (mean, standard deviation, seasonal cycle, etc.) and anomalies is 1961–1990. For simplicity, in the rest of the paper, a prime will denote the intraseasonal variables (e.g., SAT′ and z500′).

It is important to remark that the above definition of the intraseasonal scale does not remove high-frequency synoptic signals from the data. However, spectral analysis of SAT′ from each instrumental record (not shown) revealed that all of them exhibit a considerable amount of spectral power in the frequency band comprised between 30 and 90 days. Moreover, 11 out of the 16 time series (~69%) included in this study exhibit their spectral peak at periods longer than 30 days.

In section 3.4, we analyze the signal of the MJO in association with the occurrence of intraseasonal heat waves in SEPG. For that purpose, we first calculate the daily spatial SAT′ mean of the five 20CR grid points within SEPG. Then, we use that time series to detect local intraseasonal heat waves according to criteria of heat wave persistence and intensity after *Cerne and Vera* [2011]: (i) SAT′ >0 for at least five consecutive days and (ii) SAT′ larger than its own standard deviation for at least three consecutive days.

2.2. The Reconstructed MJO Index

The Wheeler and Hendon real-time multivariate MJO index, available from 1974 on, is formed by two principal components (RMM1 and RMM2) extracted from near equatorially averaged zonal wind at 850 and 200 hPa and satellite-observed OLR data. Hence, this index can be plotted on a two-dimensional phase space defined by these orthogonal axes and characterized by values of amplitude and phase, which describe the intensity and position of the convection centers in the tropical band, respectively. *Wheeler and Hendon* [2004] divided that phase space into eight equal segments and stated that the nominal time of transition between each of them is 6 days, but with variations from event to event. In this study, we use the 1905–2008 reconstruction of the MJO index of *Wheeler and Hendon* [2004] by *Oliver and Thompson* [2011]. Therefore, January–February 1905 and December 2008 are included within our period of analysis, which we call *DJF 1905–2008* for simplicity. This MJO reconstruction is based on daily fields of sea level pressure from the 20CR and was validated by its authors against several variables for three different subperiods. We define days with *active MJO phases* as those exhibiting the amplitude of their MJO index in the upper tercile of the total distribution of MJO amplitudes within DJF 1905–2008, i.e., after the exceedance of a threshold of 1.65 (dimensionless units). Although by definition all active MJO days correspond to one third of all days, the use of a common threshold for all phases partly causes slight departures from this value within each of them (see Table 2).

3. Results

3.1. The Intraseasonal Signal of SAT in Southern South America

The decomposition of SAT into the different temporal variability portions described in section 2.1 is illustrated for the temperature conditions of 22nd of January of 1992 (Figure 1). The full SAT field from 20CR shows warm conditions in the northeastern and central-eastern parts of Argentina, exceeding 37°C around 37°S, 66°W (Figure 1a). That region is located slightly to the west of the area of highest mean SAT variability (standard deviation of ~4°C). These regional warm conditions result from the superposition of the following terms: a high SAT value expected for that day of the year from the mean climatology ($>$32°C; Figure 1b), a relatively cold seasonal anomaly for the summer of 1992 (~$-$1.2°C; Figure 1c), and a warm intraseasonal anomaly detected for that particular day ($>$6°C) mainly over eastern Patagonia. The standard deviation fields of both the DJF seasonal cycle (Figure 1b) and the DJF seasonal anomalies (Figure 1c) reach their maxima in the same region as that of the full SAT field for that particular day (Figure 1a), with values on the order of 1.5°C and 2°C, respectively. Moreover, it is noteworthy that the standard deviation

Table 2. Statistics of Days Classified as Nonactive and Active MJO Phases During DJF 1905–2008

	Phase 1	Phase 2	Phase 3	Phase 4	Phase 5	Phase 6	Phase 7	Phase 8	Total
All days (% of total)	1140 (12.18)	1096 (11.71)	1344 (14.36)	1176 (12.56)	1095 (11.70)	1127 (12.04)	1189 (12.70)	1193 (12.75)	9360 (100)
Nonactive MJO days	808 [70.88]	755 [68.89]	871 [64.81]	812 [69.05]	787 [71.87]	703 [62.38]	736 [61.90]	799 [66.97]	6271 [67]
[% of each phase]	(12.88)	(12.04)	(13.89)	(12.95)	(12.55)	(11.21)	(11.74)	(12.74)	(100)
(% of total nonactive days)									
Active MJO days	332 [29.12]	341 [31.11]	473 [35.19]	364 [30.95]	308 [28.13]	424 [37.62]	453 [38.10]	394 [33.03]	3089 [33]
[% of each phase]	(10.75)	(11.04)	(15.31)	(11.78)	(9.97)	(13.73)	(14.66)	(12.75)	(100)
(% of total active MJO days)									
Number of active MJO clusters (i.e., *first days*)	94	93	112	104	96	112	115	102	-
Length of MJO clusters (median) [days]	3	4	4	3	3	4	4	3	-
Length of MJO clusters (mean) [days]	3.52	3.66	4.21	3.49	3.20	3.78	3.92	3.85	-
Length of MJO clusters (standard deviation) [days]	1.84	1.63	2.54	1.67	1.86	1.88	2.22	2.24	-

field of full SAT resembles that of SAT′ (Figure 1d). Indeed, the positive SAT′ maximum observed on our selected day (~9°C) lies within the region of highest intraseasonal variability (>3.5°C).

Therefore, this temporal decomposition of the full SAT field indicates that the largest part of the positive temperature anomaly of this particular day arises from the intraseasonal range. In fact, within SEPG (the region delimited by the red rectangle in Figure 2a), the analysis of variance of the full SAT field for DJF 1872–2010 (6.5°C^2) shows that this parameter is built in the following proportions by the different SAT

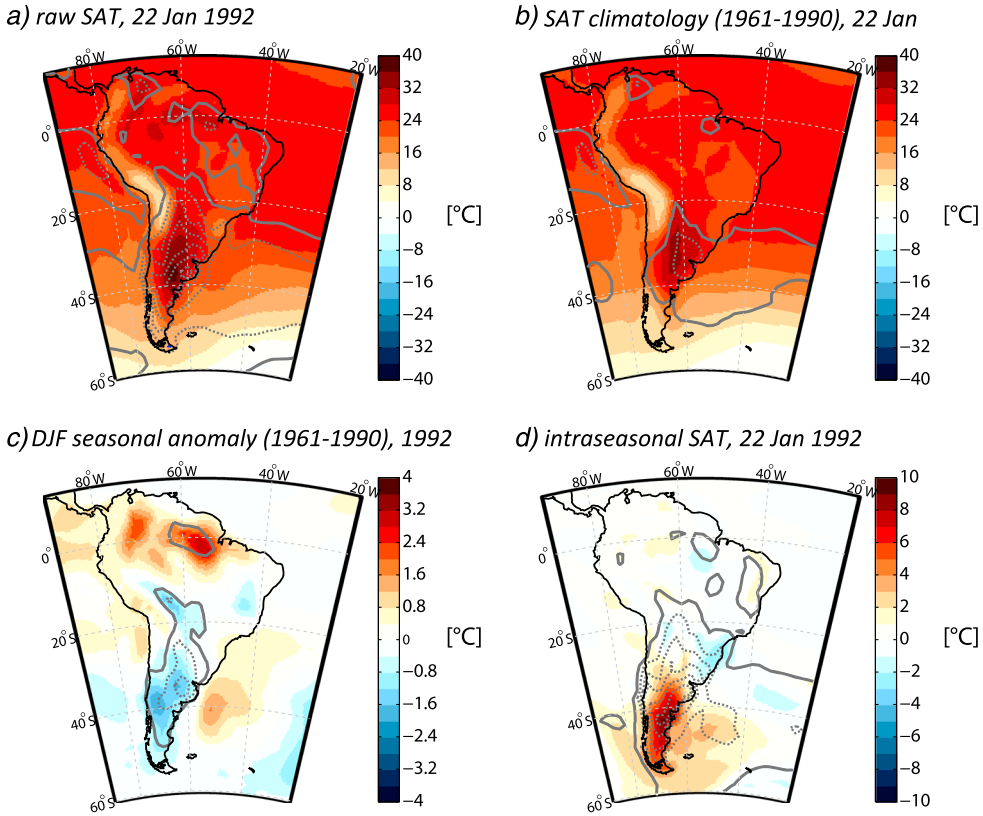

Figure 1. Decomposition of (a) the full SAT field over South America for the 22nd of January of 1992 into (b) the SAT climatology for that day (1961–1990), (c) the DJF SAT seasonal anomaly of 1992 with respect to 1961–1990, and (d) the (residual) intraseasonal SAT field for that day. Note the different color scales. The grey contours depict the 1961–1990 standard deviation of each field every 0.5°C (thin contours), starting from 1°C (thick contour). All fields correspond to 20CR.

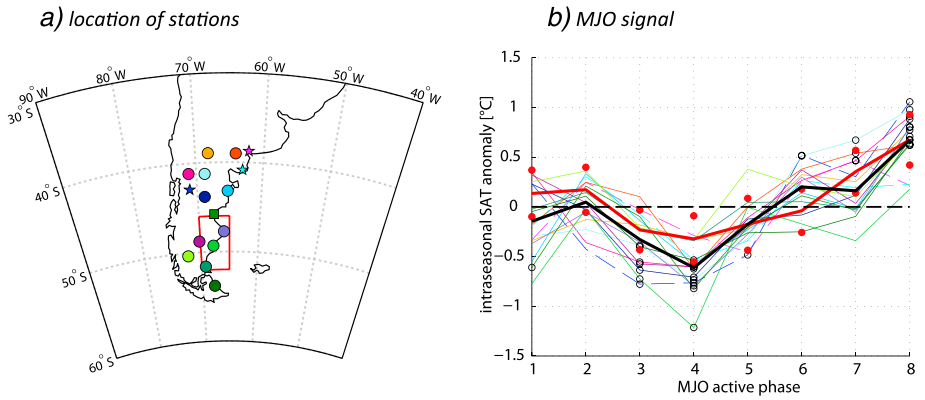

Figure 2. (a) Location of temperature stations used in this study; the red rectangle encloses southeastern Patagonia (SEPG, 46°S–52°S, 65°W–70°W). The magenta/cyan/blue stars indicate the location of Bahía Blanca/Viedma/Esquel, and the green square denotes Comodoro Rivadavia (see Table 1). (b) Composites of mean intraseasonal surface air temperature anomaly calculated for each station time series in association with active MJO phases (thin black curves), station composite mean (thick black curve), and composite mean of the five 20CR grid points within SEPG (red curve). The black circles denote statistical significance at 95% (see text); the red circles show the 95% confidence intervals for the SEPG mean signal.

components defined in section 2.1: variability of the mean seasonal cycle (~8%), variability of the seasonal mean anomalies (~14%), variability of the intraseasonal anomalies (~80%), and also by twice the covariability between the mean seasonal cycle and the intraseasonal anomalies (~ −2%). Moreover, the region enclosed by the 2°C contour of intraseasonal standard deviation (Figure 1d) comprises an extensive area spanning from the subtropics to the midlatitudes, including vast zones of Patagonia, at both sides of the Andes.

Figure S1 in the supporting information shows the SAT′ time series for DJF 1992 of the station Comodoro Rivadavia Aero in SEPG (see Table 1 and the green square in Figure 2a), along with the one extracted from 20CR (closest grid point to that station). The maximum SAT value of DJF 1992 (T_x = 37.4°C) was registered on 21 January 1992, followed by T_x = 30.3°C on 22 January 1992, our selected day. The instrumental intraseasonal anomaly T_m′ for that day reached 7.4°C, accounting for 29.6% of the measured T_m (25.1°C). The series extracted from 20CR shows a good overall agreement with the instrumental records, considering both trends and disturbances of synoptic character. However, 20CR tends to show less amplitude than the observations and thus to underestimate extreme daily values, which may be also influenced by local factors not resolved by the reanalysis.

3.2. The Modulation of Summer SAT by the MJO in Eastern Patagonia

To assess the impact of the MJO on SAT′ in Eastern Patagonia, we use T_m′ from 16 stations (Figure 2a and Table 1). For each station time series, we categorize each of the DJF days in terms of both amplitude and phase of the MJO. In the following analyses, we just consider days classified as *active* according to their MJO amplitude. Figure 2b shows a clear modulation of SAT′ by the MJO (amplitude of ~1.5°C), revealed by both the mean SAT′ of each station and the composite mean. For each station and phase, we assessed the statistical significance at 95% (two-tailed) of the mean SAT′ signal against the distribution of 1000 means calculated from random samples of the same size as that of the original group of days considered. Significant values correspond mainly to phases 3 and 4 (negative anomalies) and to 7 and 8 (positive anomalies), in agreement with the results of *Alvarez et al*. [2015]. Indeed, from the 16 analyzed stations, 13 stations (depicted by circles and a square in Figure 2a) exhibit their highest (lowest) SAT′ mean in phase 8 (4). The exceptions are Bahía Blanca (magenta star), Viedma (cyan star), and Esquel (blue star), with their maxima in phases 7/2/8 and their minima in phases 5/4/3, respectively (Table 1).

The evolution of the MJO modulation observed in the instrumental SAT′ records agrees with that revealed from the mean SAT′ signal of SEPG (the area enclosed by the red rectangle in Figure 2a) extracted from 20CR for DJF 1905–2008 (red curve in Figure 2b). This region was selected in order to make the present results comparable to those of our study about intraseasonal heat waves in the same area [*Jacques-Coper et al.*, 2015]. Although the amplitude of the signal from this region next to the Atlantic coast is lower in the

reanalysis than that in the instrumental records, a robust result is that the maximum (0.67°C) and minimum (−0.32°C) SAT′ perturbations are again detected in phases 8 and 4, respectively, giving rise to a signal amplitude of 1°C.

3.3. Large-Scale Circulation Anomalies Associated With the Extreme Signatures of the MJO on Intraseasonal SAT in Eastern Patagonia

In this section, we explore the imprint of the MJO on the SAT′ field of South America revealed by 20CR for DJF 1905–2008. We focus on the active phases of the MJO that induce the lowest and the highest SAT′ signals in Eastern Patagonia, i.e., active MJO phases 4 and 8, respectively. The figures corresponding to this section, extended to all phases, can be found in Figures S2–S4. Note that the MJO phases are not equally distributed, and thus, the relative frequencies within each phase slightly differ from the expected value of one eighth (12.5%) of all days, both for active as for nonactive MJO days, with phase 3 being the most populated in both cases (see Table 2). Because the active phases of the MJO tend to exhibit persistence, often a cluster of neighboring days that correspond to a particular active phase is observed (see Table 2 and Figure S1; again, phase 3 shows the highest persistence). In the following analyses of composites, we account for the autocorrelation effect caused by this fact by selecting just the first day of each cluster. This means that out of 364 (394) days for the active phase 4 (8), which correspond to 35.19% (33.03%) of all days within those phases (i.e., nearly one third), we retain just 104 (102) events.

Figures 3a and 3d show the midlevel intraseasonal circulation anomalies, depicted by the geopotential height at the level of 500 hPa (z500′), calculated as the composite mean of the days selected as explained above. As commented in section 2, the reader is reminded that frequencies higher than those purely belonging to the intraseasonal scale may play a role for the not-so-canonical signal of the anomalies depicted here. Nevertheless, these signals can also partly arise due to other factors, for instance, we analyze a larger period than the normally used in previous studies, our threshold for defining active MJO phases is also larger than that utilized in other works, and we "decluster" the active MJO composite; i.e., do not consider neighboring days for the construction of the composites, thus obtaining not so smooth fields as other available in the literature. In the active phase 4 (Figure 3a), convection peaks over the Maritime Continent and is suppressed in the Western Hemisphere. In the following, we focus on the geopotential anomalies observed in the Southern Hemisphere. However, the geopotential anomalies observed in the Northern Hemisphere are larger, especially over the North Pacific and North America (Figure S2d). The southern half of South America is covered by a cyclonic perturbation with a center that exceeds −45 m in magnitude, located over the southwest Atlantic. A downstream anticyclonic anomaly of similar amplitude is noticeable to its east, between southern Africa and Antarctica. Further to the east, a cyclonic (anticyclonic) anomaly appears in the southwestern (southeastern) Indian Ocean. Upstream of South America, over the South Pacific, a weak anticyclonic anomaly appears at ~70°S, 120°W, and further to the west, we observe a stronger cyclonic anomaly around 60°S, 180°. To the north of this perturbation, two anticyclonic centers are distinguished: one to the northwest (with its center located to the south of Tasmania) and the other to the northeast (centered at ~40°S, 150°W). These alternating anomalies suggest that the cyclone over the south of South America and the southwest Atlantic is part of a midlatitude wave train that extends over the South Pacific with at least partly tropical origin. The development of a Rossby wave train at 250 hPa in the South Pacific, leading to an extratropical cyclonic anomaly over the southern part of South America, was documented recently by *Alvarez et al*. [2015] between MJO phases 2 and 5 for DJF. Their results, which were made using another data set, time period, and analysis methodology as those of present paper, resemble especially the z500′ composite depicted here for phase 4 (our Figure 3a and Figure S2d). Figure 3b shows that the midlevel cyclone over southern South America is linked to a negative temperature anomaly that extends from the western coast at around 30°S until the southern tip of the continent and exceeds −1°C around the midlatitudes. To the northeast of the cold anomaly and to the southwest of a weaker anticyclonic perturbation, a warm anomaly center is evident over Uruguay and southeastern Brazil. Figure 3c exhibits the evolution of the mean SAT′ signal over SEPG (the region delimited by the red rectangle in Figure 2a) between the 10 days preceding the first day of the cluster of active phase 4 (denoted as day 0) and the 10 days after it. We note that, in general, cold conditions are found over SEPG in this composite. This result agrees with the cold anomalies over southern South America during active MJO phases 3, 4, and 5 (Figures S3c–S3e). In particular, a negative temperature anomaly is observed around the first cluster day of active phase 4. That anomaly is statistically

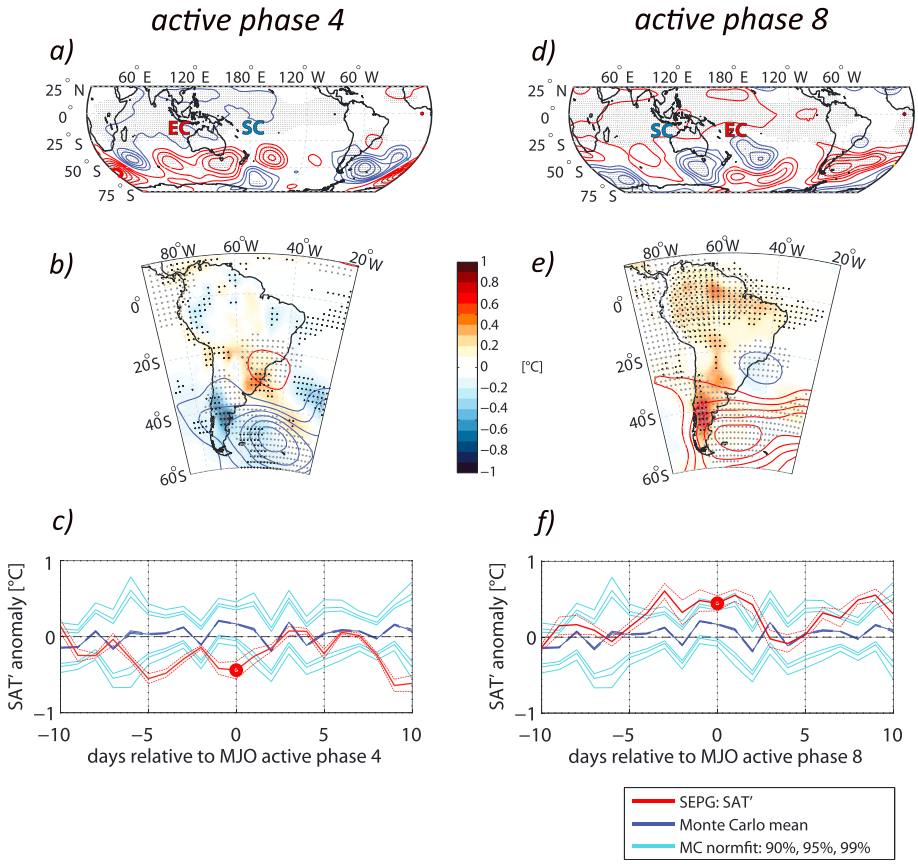

Figure 3. (a and d) Mean intraseasonal anomaly of geopotential height at 500 hPa; the red/blue contours every 7.5 m denote positive/negative anomalies, and the black dots show statistically significant values at 95%. The acronyms "SC" and "EC" stand for "suppressed convection" and "enhanced convection," respectively, and denote the location of these features with respect to the climatology for the composite of the corresponding active MJO phase. (b and e) Same fields as in the top row, superimposed on the mean intraseasonal anomaly of temperature (see color scale). The black/grey dots show statistically significant temperature/geopotential height values at 95%. (c and f) Mean intraseasonal temperature anomaly (red thick curve) and its spatial standard anomaly (thin red curves), centered on the first day of the cluster composite of the corresponding active MJO phase. The light blue lines denote the 90th, 95th, and 99th percentiles of the normal distributions adjusted to 1000 random realizations of the same size of the original sample. The panels correspond to composites of (left column) active phase 4 and (right column) active phase 8. All panels are based on 20CR for the period DJF 1905–2008.

significant at 99% after a Monte Carlo simulation of 1000 random realizations of the same size as that of the original sample.

A similar analysis was made for the active phase 8, and the resulting mean anomalies (Figure 3d) are to a great extent of opposite sign to those obtained for phase 4, also regarding the strong anomalies in the Northern Hemisphere (Figure S2h). In the active phase 8, convection is suppressed in the Maritime Continent and enhanced in the Western Hemisphere. The circulation anomalies show, in particular, a pattern of alternating z500′ of opposite sign as those of phase 4 over the South Pacific, with a more evident arch-shaped wave train-like structure extended from the date line toward South America. Again, for both phases 4 and 8, the circulation patterns described here show good agreement with those obtained by *Alvarez et al.* [2015]. The more pronounced signature for phase 8 than for phase 4 might be evidence of a stronger contribution of the tropical forcing to the development of these circulation anomalies. As discussed in next section, this hypothesis is consistent with the location of maximum convection for this MJO phase, shown by OLR, 850 hPa winds and cloud cover anomaly fields [*Wheeler and Hendon*, 2004; *Cassou*, 2008; *Oliver and Thompson*, 2011]. The downstream effect of this alternation of z500′ is an anticyclonic center located slightly to the east of Patagonia. As a consequence, warm conditions are observed over the region, with a maximum of 0.8°C at ca. 42°S in the interior of the continent (Figure 3e).

Table 3. Number of Intraseasonal Heat Waves (HW) Identified in Southeastern Patagonia on Days Classified as Nonactive and Active MJO Phases (i.e., With MJO Amplitude Below and Above 1.65, Respectively)

	Phase 1	Phase 2	Phase 3	Phase 4	Phase 5	Phase 6	Phase 7	Phase 8	Total
				DJF 1905–2008					
HW on all days (% of total)	19 (11.45)	15 (9.04)	24 (14.46)	15 (9.04)	17 (10.24)	17 (10.24)	30 (18.07)	29 (17.47)	166 (100)
HW on nonactive MJO days [% of each phase] (% of nonactive total)	14 [73.68] (12.84)	9 [60.00] (8.26)	19 [79.17] (17.43)	12 [80.00] (11.01)	11 [64.71] (10.09)	11 [64.71] (10.09)	20 [66.67] (18.35)	13 [44.83] (11.93)	109 [65.66] (100)
HW on active MJO days [% of each phase] (% of active total)	5 [26.32] (8.77)	6 [40.00] (10.53)	5 [20.83] (8.77)	3 [20.00] (5.26)	6 [35.29] (10.53)	6 [35.29] (10.53)	10 [33.33] (17.54)	16 [55.17] (28.07)	57 [34.34] (100)
				DJF 1981–2008					
HW on all days (% of total)	6 (12.50)	6 (12.50)	6 (12.50)	3 (6.25)	4 (8.33)	6 (12.50)	9 (18.75)	8 (16.67)	48 (100)
HW on nonactive MJO days [% of each phase] (% of nonactive total)	5 [83.33] (14.71)	4 [66.67] (11.76)	5 [83.33] (14.71)	3 [100] (8.82)	4 [100] (11.76)	4 [66.67] (11.76)	5 [55.56] (14.71)	4 [50.00] (11.76)	34 [70.83] (100)
HW on active MJO days [% of each phase] (% of active total)	1 [16.67] (7.14)	2 [33.33] (14.29)	1 [0] (7.14)	0 [0] (0)	0 [0] (0)	2 [33.33] (14.29)	4 [44.44] (28.57)	4 [50.00] (28.57)	14 [29.17] (100)

To the northeast, over southeastern Brazil, a cold anomaly appears in connection with a cyclonic center located above it. This feature suggests some resemblance to the SAT dipole described for warm summer means by *Jacques-Coper and Brönnimann* [2014]. In a symmetrical way to what was observed for active phase 4, the composite sequence centered on the first day of the clusters corresponding to active phase 8 (day 0; Figure 3f) bears a statistically significant positive SAT' anomaly, in particular, for day 0. The general warm conditions around day 0 agree with the composite anomaly fields of temperature for active MJO phases 7, 8, and 1 (Figures S3g, S3h, and S3a, respectively).

3.4. The Signal of the MJO in the Intraseasonal Heat Waves in Southeastern Patagonia

The 22nd of January of 1992, the day presented as an example in section 3.1, was classified as a day with an active MJO phase 8. Furthermore, on that day, a heat wave was detected over the SEPG region (the region delimited by the red rectangle in Figure 2a) using SAT' from 20CR (see Figure S1). In total, 201 intraseasonal heat waves were detected in SEPG after the criteria presented in section 2 within the period DJF 1872–2010 [*Jacques-Coper et al.*, 2015]. As in the case of active MJO phases, the days that fulfill the conditions defining a heat wave also tend to occur within clusters. Therefore, we characterize here a *heat wave event* just by the first day of such a cluster, which we name *d0*. As described in our previous work (op. cit.), the mean warm perturbation over SEPG extracted from those events lasts approximately 2 weeks and exhibits a SAT' peak of 4.3°C on *d0*. From those 201 heat waves, in this paper we use 166 events within the period that overlaps that of the reconstructed MJO index, DJF 1905–2008. From this group, we selected the 57 events that occurred during active MJO phases, that is 34.34% from the total 166 (Table 3). This amount is in agreement with what was expected from the definition of MJO active phases, namely, as the upper tercile of the MJO amplitude distribution. If we investigate the frequency distribution within each phase, we observe that heat waves tend to follow this average pattern and tend to cluster within the nonactive events (Table 3). The only exception of this behavior is found for phase 8, where 16 out of 29 heat waves (i.e., 55.17%) are detected among the active events. The spatial patterns of the mean warm anomaly induced over southern South America by the active MJO phase 8 ($n = 394\text{-}16 = 378$, excluding heat wave events) and by heat waves classified also as active MJO phase 8 ($n = 16$) are comparable (Figure S5). However, we note that by definition, the heat wave events are associated with much warmer conditions (note please the different color scales).

Considering the composite of heat wave events that are also active MJO days (i.e., *d0* is classified also as active MJO), Figure 4e and Table 4 reveal from its distribution among the MJO phases that the majority of them (16 out of 57, 28.1%, valid for DJF 1905–2008) belongs to active phase 8, followed by active phase 7 (10 out of 57, 17.5%). One should note that the expected frequency for every phase in case of a random distribution would be 7.13 events. However, as commented previously, the MJO phases are not equally distributed (see Table 2), and thus, in Figure 4 the days classified also as an active MJO event (red bars) have been normalized by the total active MJO within each phase (black dots) and shown as probability percentage values (light blue bars). Below the histogram, we show the corresponding composite fields for these events, constructed from the subset of cases that occur within 1981–2008 (Table 3). The restriction

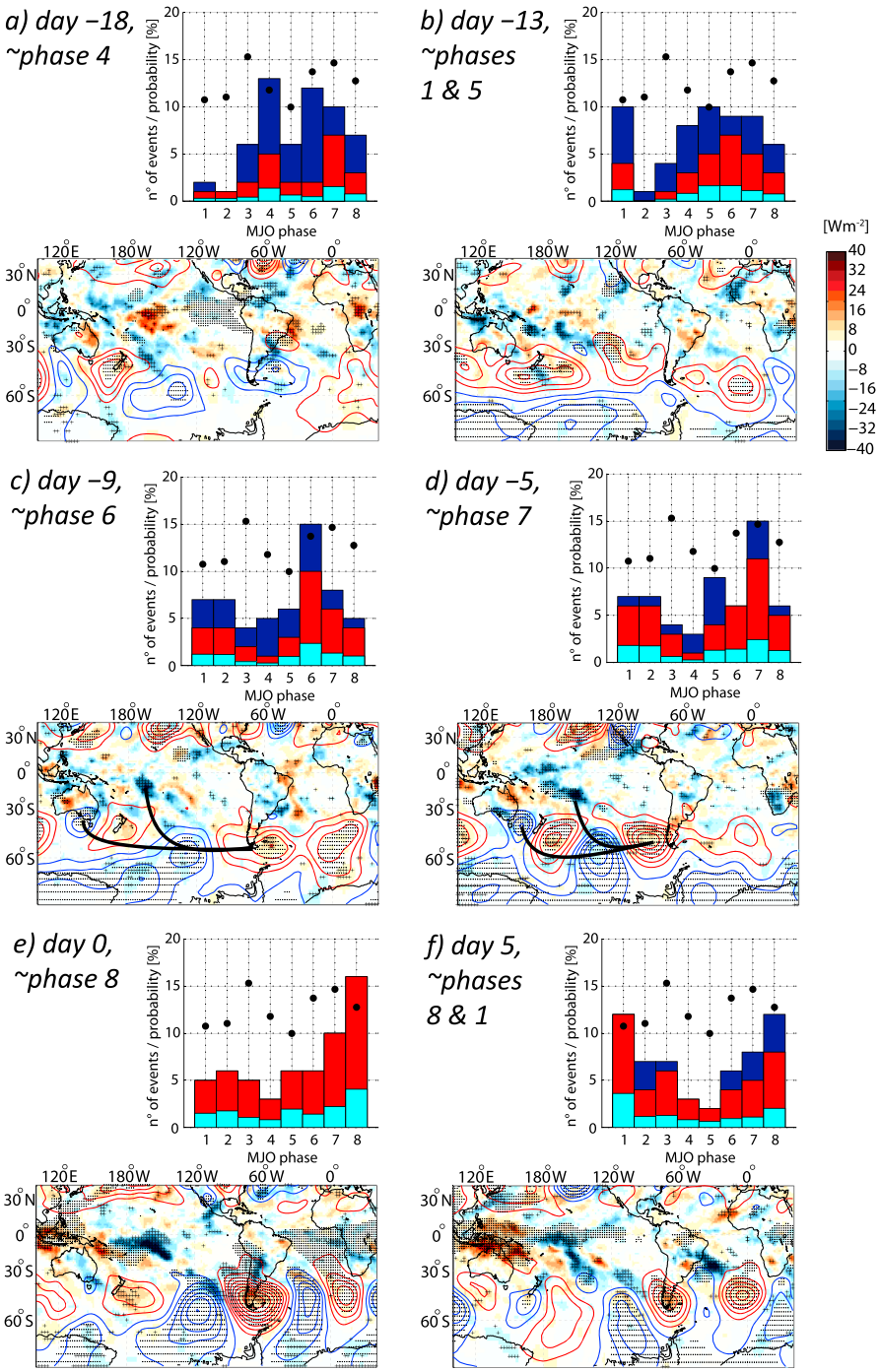

Figure 4. (top panels) Histograms of days related to the intraseasonal heat waves that occurred in southeastern Patagonia on during active MJO phases within DJF 1905–2008 (all values shown in Table 4). Panels show composites relative to *day 0*, the first day of each heat wave (*d0*), and correspond to (a) day −18, (b) day −13, (c) day −9, (d) day −5, (e) day 0, and (f) day 5. Labels indicate the most frequent phase within each composite. By definition, all MJO phases are active on *day 0* (Figure 4e), although this is not necessarily the case for the other days. The frequency of active MJO days (all days) is shown by red (dark blue) bars. The black dots indicate the relative frequency of each active MJO phase for DJF 1905–2008, in percentage (see Table 2). The light blue bars show the probability of occurrence of the MJO active days for each phase, in percentage. (bottom panels) Composite mean fields of the intraseasonal anomalies of geopotential height at 500 hPa (z500′ from 20CR, contours every 5 m, red/blue for positive/negative values) and outgoing longwave radiation (OLR′, see color scale). The spatial composite fields are constructed with the corresponding subset of data for DJF 1981–2008 (see Table 3). Statistical significance at 95% is indicated for z500′/OLR′ by black dots/crosses. In Figures 4c and 4d, the thick black lines indicate the waveguides inferred for the tropical and extratropical patterns.

Table 4. Frequency of Days Within Each MJO Phase Along the Day Sequences That Culminate in Intraseasonal Heat Waves in Southeastern Patagonia on Day 0 (*d0*), Which is Also Classified as MJO Active (see Figure 4)[a]

		Phase 1	Phase 2	Phase 3	Phase 4	Phase 5	Phase 6	Phase 7	Phase 8
Day −18	all	2	1	6	13	6	12	10	7
	active	1	1	2	5	2	2	7	3
	% active	0.30%	0.30%	0.60%	1.51%	0.60%	0.60%	*2.11%*	0.90%
Day −13	all	10	1	4	8	10	9	9	6
	active	4	0	1	3	5	7	5	3
	% active	1.20%	0.00%	0.30%	0.90%	1.51%	*2.11%*	1.51%	0.90%
Day −9	all	7	7	4	5	6	15	8	5
	active	4	4	2	1	3	10	6	4
	% active	1.20%	1.20%	0.60%	0.30%	0.90%	*3.01%*	1.81%	1.20%
Day −5	all	7	7	4	3	9	6	15	6
	active	6	6	3	1	4	6	11	5
	% active	1.81%	1.81%	0.90%	0.30%	1.20%	1.81%	*3.31%*	1.51%
Day 0	all	5	6	5	3	6	6	10	16
	active	5	6	5	3	6	6	10	16
	% active	1.51%	1.81%	1.51%	0.90%	1.81%	1.81%	3.01%	*4.82%*
Day 5	all	12	7	7	3	2	6	8	12
	active	12	4	6	3	2	4	5	8
	% active	*3.61%*	1.20%	1.81%	0.90%	0.60%	1.20%	1.51%	2.41%

[a]For each step of the sequence, all days sum 57 (the number of events considered), although not all of them belong to an active MJO phase. The percentage of active MJO phases was calculated with respect to all active MJO days for DJF 1905–2008, shown in Table 2. The highest percentage of each step of the sequence is written in italics.

of the events to the last decades is due to the limited availability of the OLR data set, which starts only in 1974. The z500′ composite of Figure 4e features a wave train-like pattern over the South Pacific, which starts in Oceania, crosses South America, and reaches South Africa. Again, as exhibited by the composite of the active MJO phase 8 in section 3.2, we observe an anticyclonic anomaly extending over the southern part of South America, whose center is located at the southwest Atlantic and exceeds 40 m. Moreover, the OLR′ field exhibits an area of significant positive anomalies over Patagonia, which may be related to fewer clouds or to a warmer than normal surface that emits more infrared radiation upwards. In the case of fewer clouds, we speculate on the possibility that enhanced solar radiation to the ground may constitute a warming factor that contributes to the occurrence of a heat wave event.

Besides, in the tropical region, the OLR′ field also features significant negative anomalies around 10°S, 160°W, a pattern that is characteristic of MJO phases 7 and 8 [*Wheeler and Hendon*, 2004; *Cassou*, 2008]. We hypothesize that the convective signal observed in the tropics is linked to the wave train-like circulation anomalies observed poleward and further to the East. As described by *Moore et al.* [2010], tropical convection can induce the formation of poleward propagating, planetary-scale Rossby waves in both hemispheres, a phenomenon that is called the Matsuno-Gill response [*Matsuno*, 1966; *Gill*, 1980; *Barlow et al.*, 2007]. In fact, *Alvarez et al.* [2015] described for DJF the development of a Rossby wave train at 250 hPa in the South Pacific between phases 6 and 1 in association with the tropical upper level divergent circulation anomaly caused by the MJO heating anomaly in the Indian Ocean-Western Pacific region and related this circulation pattern to the anticyclonic anomaly in the southern tip of South America.

To further explore this feature, in Figure 4 we also show the composite fields of the days preceding *d0*. Note that although all days corresponding to *d0* are classified by definition as active MJO phases (red bars), this is not necessarily the case for the rest of the days. However, the MJO reconstruction still provides a classification according to MJO phases for all available days. The histogram of day −5 (Figure 4d and Table 4) shows its highest frequency of events in phase 7 (15 out of 57, 26.3%, valid for DJF 1905–2008), a value that doubles again the one expected from a random distribution. Considering that the nominal duration of each MJO phase is 6 days [*Wheeler and Hendon*, 2004], this result seems to be a natural consequence of the distribution observed for the *d0* composite. In the corresponding z500′ composite (valid for DJF 1981–2008), shown below, an arch-shaped alternation of negative and positive anomaly centers is located over the South Pacific. The connection between this anomalous circulation pattern and the negative OLR′ anomaly located around 15°S, 160°W appears evident in this panel, in such a way that deep tropical convection seems to

trigger, at least partly, the wave train observed downstream. However, the cyclone located over the Tasman Sea, between Australia and New Zealand, suggests that the wave train pattern also extends further to the southwest of the tropical convective anomaly. Thus, the wave train pattern seems to bear also the signal of a midlatitude disturbance. Therefore, these anomalies lead us to hypothesize that the observed wave train pattern may arise from a constructive tropical-extratropical interaction, as indicated by the waveguides drawn in Figures 4c and 4d (thick black lines).

In the composite of day −9 relative to *d0* (Figure 4c and Table 4), again 15 out of 57 days (26.3%, valid for DJF 1905–2008) correspond to MJO phase 6. In this case, the tropical convective anomaly mentioned above is located closer to the date line. The corresponding anomalies of the z500′ field, which are weaker than in the composites discussed previously, still resemble the wave train-like structure over the South Pacific. On day −13 (Figure 4b and Table 4), despite the fact that the frequency distribution looks more uniform, phases 1 and 5 are more populated than the others, both with 10 out of 57 events (17.5%, valid for DJF 1905–2008). On day −18 (Figure 4a and Table 4), most of the events are classified as phase 4 (13 out of 57, 22.8%, valid for DJF 1905–2008). In this case, the cyclonic anomaly over southern South America and the southwest Atlantic corresponds to that discussed in section 3.2 for cold conditions in Patagonia. For both composites of day −13 and day −18, tropical convection is mainly found over the Maritime Continent, a result which is consistent with predominating MJO phases 5 and 4, respectively.

The sequence revealed by these composites indicates that the occurrence of the selected heat wave events tend to follow the development of the MJO. This fact means that there is a time lag between the large-scale wave propagation and the occurrence of a heat wave in SEPG. This result is clearly depicted by the 21 day long trajectories of these heat wave events, drawn on the MJO phase space diagrams, along with the heat wave events peaking in the rest of the active MJO phases (Figure S6). The present result suggests that the mere MJO may induce considerable temperature perturbations on the summer climate of Patagonia, even beyond the mere SAT modulation shown previously. A relevant remark concerning predictability is, however, that not all days from a sequence culminating in a heat wave in SEPG on *d0* are classified as MJO active. In Table 4 and Figure 4, we explicitly show at each step of the sequence the information related to the occurrence of a heat wave event on *d0* that is provided by the active MJO days, in the form of percentages. Thus, we notice that the most frequent phases considering just active MJO days are phase 7 for day −18, phase 6 for days −13 and −9, phase 7 for day −5, phase 8 for day 0 (*d0*), and phase 1 for day 5.

The eastward propagation of the circulation patterns observed in the sequence of composites of Figure 4 is further supported by the frequency of phases of day +5 (Figure 4f and Table 4), where most members are found in phases 8 and 1, each of them with 12 occurrences out of 57 (21.1%, valid for DJF 1905–2008). Although by this day the large-scale wave train pattern of z500′ over the South Pacific has already weakened, a positive OLR′ signal is still observed over Patagonia. A further feature of this composite is the enhanced convective activity observed in the South Atlantic Convergence Zone in southeastern Brazil, a phenomenon observed in our previous work on intraseasonal heat waves in SEPG and also at the seasonal scale for summer [*Jacques-Coper and Brönnimann*, 2014].

Figure S7 shows analogous composites of Figure 4, but considering the intraseasonal anomalies of the wind at 200 hPa and of the streamfunction at 200 hPa. The corresponding panels essentially reveal that the wave train pattern found in z500′, leading to the heat wave in SEPG on *d0*, can also be identified in upper levels, especially in the composites of days −5 and 0 relative to *d0* (Figures 4d and 4e). Thus, the large-scale circulation anomalies causing heat waves in SEPG are present throughout the troposphere. In particular, for day −5, a noteworthy anticyclonic anomaly is found to the south of the main tropical convection center in the western Pacific.

3.5. An Example of Tropical-Extratropical Interaction: The Case Study of the 22nd of January 1992

To better understand the interaction between tropical convection and the extratropical dynamics, in the following we analyze in detail selected development stages of the 6-hourly large-scale circulation anomaly that leads to the heat wave in SEPG on the 22nd of January 1992, as depicted by 20CR. We are aware that only by means of a modeling study it would be possible to discern between tropical and extratropical waves. However, following descriptions can shed light on the subject under analysis.

Ten days before the event, on the 12th of January (classified as *active MJO phase 7*; Figure 5a and Figure S1), an alternation of z500′ centers is observed around 50°S, with cyclones to the south of Australia and at 60°S,

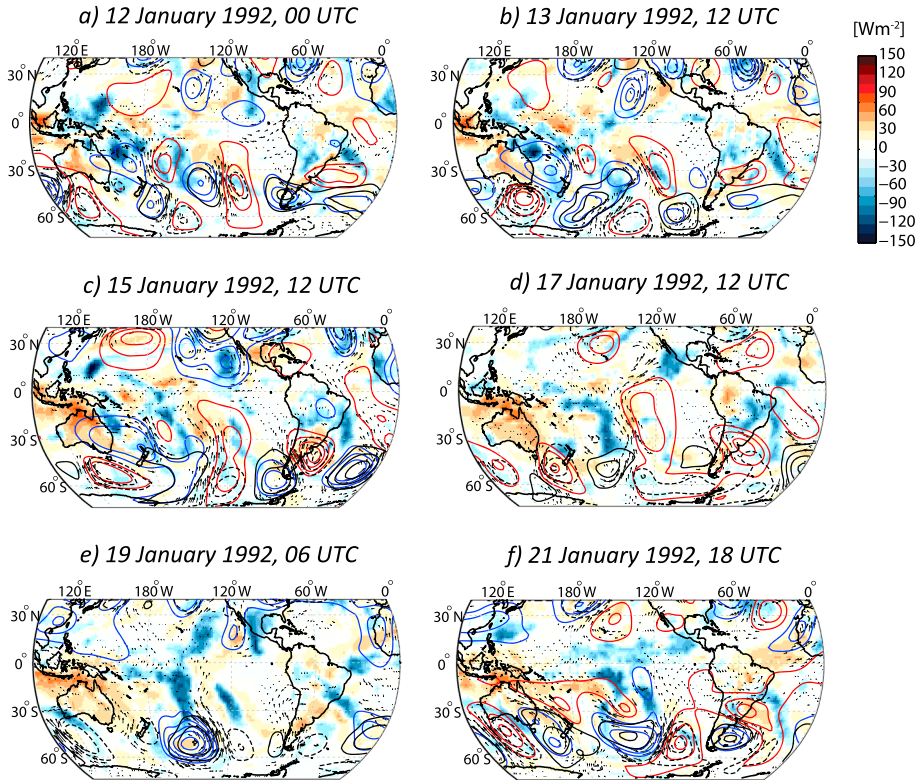

Figure 5. Case study of the heat wave of 22nd of January 1992, based on 20CR. Selected fields of the 6-hourly sequence within the 10 days preceding the event are shown: (a) 12th of January 1992, 00:00 UTC; (b) 13th of January 1992, 12:00 UTC; (c) 15th of January 1992, 12:00 UTC; (d) 17th of January 1992, 12:00 UTC; (e) 19th of January 1992, 06:00 UTC; and (f) 21st of January 1992, 18:00 UTC. The fields correspond to the intraseasonal anomalies of outgoing longwave radiation (shaded, see color scale), geopotential height at 500 hPa (continuous/dashed contours every 100 m for positive/negative values) and wind at 200 hPa. Wind vectors are only shown where the upper tercile of the intensity distribution of the zonal or the meridional component of the wind at 200 hPa during January 1992 is exceeded. The streamfunction at 200 hPa (red/blue contours every 10^7 m^2/s for positive/negative values) was calculated from the corresponding intraseasonal anomalies of the wind components. Zero contours omitted.

160°W, and anticyclones to the south of New Zealand (around the date line), also at 40°S, 130°W, and over southern South America. This structure, noticeable also in the intraseasonal wind anomalies at 200 hPa (wnd200′) and their streamfunction (sf200′), resembles a *midlatitude wave train pattern*. In the tropical Pacific, the main convective activity is located to the north and to the east of Australia, at ~15°N, 150°E and 20°S, 170°E, respectively. Directly poleward of these convective clusters, upper air divergence induces anticyclonic anomalies, which are thereafter called *tropical anomalies*.

Nine days before the event, on the 13th of January (classified as *active MJO phase 7*; Figure 5b), the midlatitude wave train has propagated eastward with respect to the preceding day. The tropical convective activity is more restricted to the east of Australia, and the associated upper level anticyclonic center appears to its southeast, centered at ~30°S, 170°E.

One week before the event, on the 15th of January (classified as *active MJO phase 8*; Figure 5c), the alternation of negative and positive anomalies in the midlatitude wave train of the Southern Hemisphere is evident. In particular, an anticyclone is identified west of the southern tip of South America, which is presumably responsible for the cold anomalies in Eastern Patagonia (Figure S1) by advecting air form the southeast. The main tropical convective center is located around 15°S, 170°W. The sf200′ field reveals extratropical anticyclonic circulation patterns to the west of this longitude in both hemispheres. In the South Hemisphere, the streamfunction contours connect the corresponding anticyclone with that of the midlatitude wave train. From this fact, we speculate that there may be a constructive superposition of tropical and extratropical circulation anomalies.

On day −5, the 17th of January (classified as *active MJO phase 8*; Figure 5d), the convective activity in the central-western Pacific has intensified. Apparently in association with this large-scale convection center, southerly wind anomalies at 200 hPa are observed in the south Pacific along 140°W. The action centers of the midlatitude wave train have propagated eastward with respect to the last composite. On this day, a cyclonic circulation over the Tasman Sea appears to be related to a positive (negative) OLR′ anomaly over eastern Australia (the North Island of New Zealand). See *Jacques-Coper et al.* [2015] for a discussion on that. The anticyclonic anomaly south of the tropical convective center, however, remains quite stationary, centered at ~45°S, 160°W.

Three days before the event, on the 19th of January (classified as *active MJO phase 8*; Figure 5e), both the main convection center in the subtropics and the associated midlatitude anticyclone have strengthened, along with southerly wnd200′ at ~140°W. To the east of that anticyclone, a cyclone-anticyclone-cyclone alternation can be observed, with the easternmost anticyclone approaching the southern tip of South America.

On the day previous to the event, the 21st of January (classified as *active MJO phase 8*; Figure 5f), the tropical convective cell, by then in the central Pacific, is spatially more restricted. On that day, this convective anomaly, along with the midlatitude wave train, has shifted to the east. In this way, a strengthened cyclone is located to the west of southern South America and an anticyclone is evident over Patagonia and the southwest Atlantic. As discussed in previous sections, this anticyclonic circulation is related to the warm anomaly in Eastern Patagonia (and SEPG, in particular).

It is interesting to note that the day-to-day development of the circulation anomalies over the southern Pacific strongly resembles the composite pattern shown in this study (Figure 4 and Figure S7). Moreover, in particular, the midlatitude disturbances show good agreement in time and space with the pattern proposed by our previous work on intraseasonal heat waves in SEPG [*Jacques-Coper et al.*, 2015] and with that associated with the MJO influence over South America [e.g., *Alvarez et al.*, 2015]. The case study described above provides then good insight into the way in which the circulation anomalies related to tropical convective activity can influence the midlatitude wave train by interacting constructively.

4. Discussions and Conclusions

In this work, we have explored the modulation of intraseasonal SAT in Eastern Patagonia by the Madden-Julian Oscillation (MJO). The study is based on long-term climate reconstructions, namely, the Twentieth Century Reanalysis (20CR) and the reconstruction provided by *Oliver and Thompson* [2011] of the MJO index defined by *Wheeler and Hendon* [2004] for 1905–2008, based on the SLP fields from 20CR. We complement our analysis with instrumental daily records of surface air temperature (SAT) from Eastern Patagonia, from which the majority starts in DJF 1957. Hence, an effort has been made to use the longest data sets available in order to extract robust relationships between them.

We found that the intraseasonal component of instrumental SAT in Eastern Patagonia exhibits a signal induced by the active phases of the MJO. In particular, for most of the stations, warm (cold) conditions are statistically significant at 95% during active phases 7 and 8 (3 and 4). A robust result is that most instrumental records show their warmest departure (ranging mostly between 0.5°C and 1°C) for active phase 8 and their coldest anomaly (mostly between −0.5°C and −1°C) for active phase 4. The exceptions of Bahía Blanca and Viedma (minimum during active phase 5 (4) and maximum during active phase 7 (2), respectively) are not statistically significant at 95% using a Monte Carlo distribution from 1000 random realizations and may be explained by the influence of rather local effects. Nonetheless, the minimum at phase 5 of Bahía Blanca and the maximum at phase 2 of Viedma are plausible when compared to the regional fields depicted in Figure S3, which show coherent regional cold and warm anomalies, respectively, around the corresponding stations. Esquel, the third exception (minimum during active phase 3 and maximum during active phase 8) shows a difference between its mean temperatures during active phase 3 and active phase 4 that is actually less than the expected from said random distributions (at the 95% confidence level). However, its minimum during active phase 3 may be due to its location, further to the west than most of the stations (see our Figure S3c and Figure 7 from *Alvarez et al.* [2015]). All in all, we present here an overall intraseasonal modulation of ~1.5°C of amplitude across Eastern Patagonia (Figure 2b). In 20CR, the modulation of SAT in southeastern Patagonia (SEPG, the region delimited by the red rectangle in Figure 2a) features a lower amplitude of the signal, of around 1°C, but also shows its extreme values in active MJO phases 4 and 8. Therefore, we restricted our analysis to those two specific

MJO phases. The corresponding SAT anomalies induced by them in SEPG seem to last for a couple of days around the first day of each cluster of active MJO phases (Figures 3c and 3f).

The consistency of the present results suggests that there may be an enhanced predictability of summer intraseasonal SAT in Eastern Patagonia, subject to a skillful MJO forecasting capability, which is estimated to be up to 15–17 days [*Seo et al*., 2009]. Indeed, the geographical distribution and temporal evolution of tropical moist deep convection determines the prediction of midlatitude weather at lead times longer than 4 or 5 days [*Lau et al*., 2012, and references therein]. In this sense, the present results provide an alternative perspective on the predictability of the intraseasonal component of summer SAT in Patagonia. This conclusion stands out, in agreement with the recent results of *Alvarez et al*. [2015], and in spite of previous related findings, which showed that the mutual information between SAT and the MJO is highest not in Patagonia but in southeastern Brazil and northeastern Argentina, and features its maximum in autumn and winter and its minimum in summer [*Naumann and Vargas*, 2010].

Concerning the regional- and large-scale circulation patterns associated with the MJO signal in Eastern Patagonia, we found that positive (negative) SAT anomalies are linked to a midlevel anticyclonic (cyclonic) circulation anomaly centered over the southwest Atlantic and extending over southern South America, in agreement with previous work on regional summer SAT means [*Jacques-Coper and Brönnimann*, 2014]. Moreover, these circulation anomalies appear to be part of patterns of alternating polarities of the intraseasonal component of geopotential height in 500 hPa over the South Pacific. Furthermore, for active phases 4 and 8, these patterns show almost opposite anomalies.

The exploration of the links between the development of heat waves in SEPG and the active MJO allows us to conclude that although the majority of the heat waves occur on nonactive MJO days (109 out of 166 events, 65.66%), this pattern exceptionally changes for phase 8 (just 13 out of 29 events, 44.83%). In other words, most of the heat waves within phase 8 correspond to active MJO events (16 out of 29, 55.17%). Based on a contingency table, we found that the difference between this distribution and one obtained by chance is statistically significant at the 95% confidence level (chi-square test). Moreover, regarding just active MJO phases, we found that the observed distribution of heat waves is also statistically different from one expected by chance at a confidence level of 95% (chi-square test). Furthermore, the heat waves tend to culminate in phase 8 (16 out of 57, 28.07%; Figure 4e).

The previous results are consistent with the maximum SAT′ anomaly detected for active phase 8 in the analyzed instrumental network. A direct comparison of the evolution of the circulation anomalies with those of convective activity in the tropics suggests a possible role of the MJO in the triggering of heat waves in SEPG. Our findings insinuate that the arched wave train pattern over the South Pacific observed for the active phase 8 is associated with an area of enhanced convection in the tropics, located around 10°S, 160°W, which is characteristic of that phase [*Wheeler and Hendon*, 2004; *Cassou*, 2008]. The proposed association between tropical convection and the downstream development of an alternation of circulation anomalies is supported by the fields of composites corresponding to 5 and 9 days preceding a heat wave in SEPG, identified as MJO phases 7 and 6, respectively (Figures 4c and 4d).

To illustrate our results, we selected DJF 1992. The MJO modulation of the spatial mean intraseasonal temperature in Eastern Patagonia is clearly observed in the intraseasonal development of the measured and reconstructed temperature in Comodoro Rivadavia Aero (45°47′S, 67°30′W; Figure 2a and Figure S1). The corresponding series extracted from 20CR reaches its maximum around the 22nd of January, with a positive (negative) trend before (after) it. The 22nd of January 1992 was classified as active MJO phase 8 and also identified as the first day of a heat wave in SEPG. We showed that the largest part of the temperature anomaly for that maximum value was consequence of the intraseasonal variability. The description of the development of the large-scale intraseasonal circulation anomalies for the 10 days preceding that event provided an insight into the possible constructive interaction between tropical convective activity and the midlatitude wave train.

Therefore, a main conclusion of the present work, which may be used as a hypothesis for further research, is that midlatitude disturbances resulting from extratropical dynamics leading to SAT impacts in Patagonia may interact with tropical activity in a way of constructive interference in order to enhance the probability of occurrence of a heat wave, in particular, in the subregion SEPG. In other words, we suggest that this is a case of a profound association between a tropical intraseasonal oscillation and the disturbances

embedded in the midlatitudes, as described in *Lau et al*. [2012] and shown in previous works [e.g., *Matthews*, 2004; *Yoo et al*., 2011]. This suggestion is based on the fact that heat waves may occur in all active MJO phases but clearly tend to be favored by the conditions set up mainly by active phase 8. Regarding the predictability of these phenomena, we observe from Table 4 that the probability of occurrence of a heat wave in SEPG on an active MJO phase 8 (day 0) is 4.82%, more than twice the value observed for MJO active phases 1–6. Moreover, 9 days in advance of such an event, given an active MJO phase 6, there is still a probability of 3.01% for the occurrence of a heat wave on day 0. These values, although low, are in the order of extreme phenomena related to the MJO, such as extreme floods in the Philippines [*Zhang*, 2013], and constitute valuable information for forecasting purposes based on the state of the MJO. In line with our findings, it is worth mentioning that at the intraseasonal scale, convection in the South Pacific Convergence Zone (SPCZ) is significantly enhanced during MJO phases 5, 6, and 7 [*Matthews*, 2012], a result that agrees with the timing shown by our results. Also, *Nogués-Paegle and Mo* [1997] identified a SPCZ influence onto the climate variability in southern South America on intraseasonal time scales. Hence, this MJO-related feature may also be explored as a further source of circulation anomalies in the South Pacific and, in particular, of predictability of heat waves in Patagonia. However, although this predictability is enhanced by the temperature background state set up by the MJO, there are also factors that limit it. For instance, the observed constructive interference between the MJO-induced circulation anomalies and other wave-like circulation perturbations seems to indicate that a skillful forecast of the MJO state may not be enough as a predictor. This fact is reflected in the low frequency of occurrence of these extreme events when sorted after the active MJO phases (Figure 4). For a better forecast skill, further predictors should be explored, in both the large spatial scale (e.g., other *background* climate modes that could interact with the MJO) and the regional scale (e.g., soil properties such as water content). In this sense, one should note that the MJO is not the only source for intraseasonal and subseasonal oscillations in high latitudes of the Southern Hemisphere [*Ghil and Mo*, 1991; *Gonzalez et al*., 2014], and hence, heat waves over Eastern Patagonia may be also related to other factors that, in particular, can favor blocking and warm conditions in this region. From a climatological perspective, the positive phase of the Southern Annular Mode (SAM) is related to roughly zonal anticyclonic anomalies over Patagonia and thus warm regional conditions [*Gillett et al*., 2006; *Garreaud et al*., 2009], whereas warm anomalies are also enhanced by El Niño conditions [*Garreaud et al*., 2009]. For the intraseasonal time scale during the warm season, *Carvalho et al*. [2005] observed that positive SAM events showed concomitant negative OLR anomalies near the date line, and *Flatau and Kim* [2012] found that negative SAM states are related to MJO phases 1–4. These results are in agreement with our present findings. With focus on daily variability, the combined effect of SAM and the El Niño–Southern Oscillation was shown to modify the blocking frequency in the Southern Hemisphere, at least during winter [*Oliveira et al*., 2014]. Further research should explore the possible implications of these factors on the occurrence of heat waves in Eastern Patagonia.

Using long-term observations and reconstructions, we have presented robust evidence for a tropical influence influence behind the evolution of the observed circulation patterns leading to strong temperature perturbations in Eastern Patagonia. Further efforts are needed to investigate this subject through modeling experiments. In fact, an atmospheric response comparable to that observed for the composite of day −9 with respect to the occurrence of a heat wave in SEPG (classified as mostly MJO phase 6; Figure 4c), although of different phasing, was simulated by *Ding et al*. [2011] for austral winter as a consequence of an anomalous warm sea surface temperature pattern in the central Pacific.

Acknowledgments

Twentieth Century Reanalysis V2 and Interpolated OLR data were obtained from the NOAA/OAR/ESRL PSD Web site (http://www.esrl.noaa.gov/psd/). The observational temperature data set was supplied by the Argentinean National Weather Service. The authors thank the availability of the reconstructed MJO index calculated by E.C.J. Oliver and K.R. Thompson and provided by Eric C.J. Oliver on his personal Web page (http://passage.phys.ocean.dal.ca/~olivere/histmjo.html). M.J.C. acknowledges the CLIMANDES project (SDC, Switzerland) and the BecasChile scholarship program (Comisión Nacional de Investigación Científica y Tecnológica de Chile, CONICYT). C.V. and B.C. acknowledge the ANPCyT PICT-2010-2110 Project (Argentina). We thank Alexander Stickler and Aldo Montecinos for their useful comments, Paraskevi Giannakaki for the technical support, and Brant Liebmann and two anonymous reviewers, whose comments greatly helped to improve the original manuscript.

References

Alvarez, M., C. S. Vera, G. N. Kiladis, and B. Liebmann (2015), Influence of the Madden Julian Oscillation on precipitation and surface air temperature in South America, *Clim. Dyn.*, doi:10.1007/s00382-015-2581-6.

Barlow, M., A. Hoell, and F. Colby (2007), Examining the wintertime response to tropical convection over the Indian Ocean by modifying convective heating in a full atmospheric model, *Geophys. Res. Lett.*, *34*, L19702, doi:10.1029/2007GL030043.

Barrett, B. S., J. F. Carrasco, and A. P. Testino (2011), Madden–Julian Oscillation (MJO) modulation of atmospheric circulation and Chilean winter precipitation, *J. Clim.*, *25*(5), 1678–1688, doi:10.1175/JCLI-D-11-00216.1.

Berman, A., G. Silvestri, and R. Compagnucci (2013), On the variability of seasonal temperature in southern South America, *Clim. Dyn.*, *40*(7–8), 1863–1878, doi:10.1007/s00382-012-1596-5.

Carvalho, L. M. V., C. Jones, and T. Ambrizzi (2005), Opposite phases of the Antarctic oscillation and relationships with intraseasonal to interannual activity in the tropics during the austral summer, *J. Clim.*, *18*(5), 702–718, doi:10.1175/JCLI-3284.1.

Cassou, C. (2008), Intraseasonal interaction between the Madden-Julian Oscillation and the North Atlantic Oscillation, *Nature*, *455*(7212), 523–527.

Cerne, S. B., and C. S. Vera (2011), Influence of the intraseasonal variability on heat waves in subtropical South America, *Clim. Dyn.*, *36*(11–12), 2265–2277, doi:10.1007/s00382-010-0812-4.
Compo, G. P., et al. (2011), The Twentieth Century Reanalysis Project, *Q. J. R. Meteorol. Soc.*, *137*(654), 1–28, doi:10.1002/qj.776.
Coronato, F., and A. Bisigato (1998), A temperature pattern classification in Patagonia, *Int. J. Climatol.*, *18*(7), 765–773, doi:10.1002/(SICI)1097-0088(19980615)18:7<765::AID-JOC282>3.0.CO;2-H.
Del Valle, H. F., N. O. Elissalde, D. A. Gagliardini, and J. Milovich (1998), Status of desertification in the Patagonian region: Assessment and mapping from satellite imagery, *Arid Soil Res. Rehabil.*, *12*(2), 95–121, doi:10.1080/15324989809381502.
Ding, Q., E. J. Steig, D. S. Battisti, and M. Kuttel (2011), Winter warming in West Antarctica caused by central tropical Pacific warming, *Nat. Geosci.*, *4*(6), 398–403.
Donald, A., H. Meinke, B. Power, A. de H. N. Maia, M. C. Wheeler, N. White, R. C. Stone, and J. Ribbe (2006), Near-global impact of the Madden-Julian Oscillation on rainfall, *Geophys. Res. Lett.*, *33*, L09704, doi:10.1029/2005GL025155.
Dussaillant, A., G. Benito, W. Buytaert, P. Carling, C. Meier, and F. Espinoza (2010), Repeated glacial-lake outburst floods in Patagonia: An increasing hazard?, *Nat. Hazards*, *54*(2), 469–481, doi:10.1007/s11069-009-9479-8.
Flatau, M., and Y.-J. Kim (2012), Interaction between the MJO and polar circulations, *J. Clim.*, *26*(11), 3562–3574, doi:10.1175/JCLI-D-11-00508.1.
Garreaud, R. D., M. Vuille, R. Compagnucci, and J. Marengo (2009), Present-day South American climate, *Palaeogeogr. Palaeoclimatol. Palaeoecol.*, *281*(3–4), 180–195, doi:10.1016/j.palaeo.2007.10.032.
Garreaud, R., P. Lopez, M. Minvielle, and M. Rojas (2012), Large-scale control on the Patagonian climate, *J. Clim.*, *26*(1), 215–230, doi:10.1175/JCLI-D-12-00001.1.
Ghil, M., and K. Mo (1991), Intraseasonal oscillations in the global atmosphere. Part II: Southern Hemisphere, *J. Atmos. Sci.*, *48*(5), 780–790, doi:10.1175/1520-0469(1991)048<0780:IOITGA>2.0.CO;2.
Gill, A. E. (1980), Some simple solutions for heat-induced tropical circulation, *Q. J. R. Meteorol. Soc.*, *106*(449), 447–462, doi:10.1002/qj.49710644905.
Gillett, N. P., T. D. Kell, and P. D. Jones (2006), Regional climate impacts of the Southern Annular Mode, *Geophys. Res. Lett.*, *33*, L23704, doi:10.1029/2006GL027721.
Gonzalez, P. M., L. Polvani, R. Seager, and G. P. Correa (2014), Stratospheric ozone depletion: A key driver of recent precipitation trends in South Eastern South America, *Clim. Dyn.*, *42*(7–8), 1775–1792, doi:10.1007/s00382-013-1777-x.
Jacques-Coper, M., and S. Brönnimann (2014), Summer temperature in the eastern part of southern South America: Its variability in the twentieth century and a teleconnection with Oceania, *Clim. Dyn.*, *43*(7–8), 2111–2130, doi:10.1007/s00382-013-2038-8.
Jacques-Coper, M., S. Brönnimann, O. Martius, C. S. Vera, and B. Cerne (2015), Summer heat waves in Southeastern Patagonia: An analysis of the intraseasonal timescale, *Int. J. Climatol.*, in press.
Juliá, C., D. A. Rahn, and J. A. Rutllant (2012), Assessing the influence of the MJO on strong precipitation events in subtropical, semi-arid north-central Chile (30°S), *J. Clim.*, *25*(20), 7003–7013, doi:10.1175/JCLI-D-11-00679.1.
Kanamori, H., T. Yasunari, and K. Kuraji (2013), Modulation of the diurnal cycle of rainfall associated with the MJO observed by a dense hourly rain gauge network at Sarawak, Borneo, *J. Clim.*, *26*(13), 4858–4875, doi:10.1175/JCLI-D-12-00158.1.
Kargel, J. S., et al. (2012), Glaciers in Patagonia: Controversy and prospects, *Eos, Trans. AGU*, *93*(22), 212, doi:10.1029/2012EO220011.
Lau, W. M., D. Waliser, and P. Roundy (2012), Tropical–extratropical interactions, in *Intraseasonal Variability in the Atmosphere–Ocean Climate System SE - 14*, pp. 497–512, Springer, Heidelberg.
Liebmann, B., and C. A. Smith (1996), Description of a complete (interpolated) outgoing longwave radiation dataset, *Bull. Am. Meteorol. Soc.*, *77*, 1275–1277.
Madden, R. A., and P. R. Julian (1971), Detection of a 40–50 day oscillation in the zonal wind in the tropical Pacific, *J. Atmos. Sci.*, *28*(5), 702–708, doi:10.1175/1520-0469(1971)028<0702:DOADOI>2.0.CO;2.
Maloney, E. D., and J. T. Kiehl (2002), MJO-Related SST variations over the tropical eastern Pacific during Northern Hemisphere summer, *J. Clim.*, *15*(6), 675–689, doi:10.1175/1520-0442(2002)015<0675:MRSVOT>2.0.CO;2.
Matsuno, T. (1966), Quasi-geostrophic motions in the equatorial area, *J. Meteorol. Soc. Jpn. Ser. II*, *44*(1), 25–43.
Matthews, A. J. (2004), Variability of Antarctic circumpolar transport and the Southern Annular Mode associated with the Madden-Julian Oscillation, *Geophys. Res. Lett.*, *31*, L24312, doi:10.1029/2004GL021666.
Matthews, A. J. (2012), A multiscale framework for the origin and variability of the South Pacific Convergence Zone, *Q. J. R. Meteorol. Soc.*, *138*(666), 1165–1178, doi:10.1002/qj.1870.
Matthews, A. J., G. Pickup, S. C. Peatman, P. Clews, and J. Martin (2013), The effect of the Madden-Julian Oscillation on station rainfall and river level in the Fly River system, Papua New Guinea, *J. Geophys. Res. Atmos.*, *118*, 10,910–926,935, doi:10.1002/jgrd.50865.
Mazzonia, E., and M. Vazquez (2009), Desertification in Patagonia, in *Natural Hazards and Human-Exacerbated Disasters in Latin America*, E. S. Processes, vol. 13, edited by E. G. Latrubesse, pp. 351–377, Elsevier, Amsterdam.
Mo, K. C., and J. N. Paegle (2001), The Pacific–South American modes and their downstream effects, *Int. J. Climatol.*, *21*(10), 1211–1229, doi:10.1002/joc.685.
Moore, R. W., O. Martius, and T. Spengler (2010), The Modulation of the subtropical and extratropical atmosphere in the Pacific Basin in response to the Madden–Julian Oscillation, *Mon. Weather Rev.*, *138*(7), 2761–2779, doi:10.1175/2010MWR3194.1.
Naumann, G., and W. M. Vargas (2010), Joint diagnostic of the surface air temperature in southern South America and the Madden–Julian Oscillation, *Weather Forecasting*, *25*(4), 1275–1280, doi:10.1175/2010WAF2222418.1.
Naumann, G., and W. M. Vargas (2012), A study of intraseasonal temperature variability in southeastern South America, *J. Clim.*, *25*(17), 5892–5903, doi:10.1175/JCLI-D-11-00482.1.
Nogués-Paegle, J., and K. C. Mo (1997), Alternating wet and dry conditions over South America during summer, *Mon. Weather Rev.*, *125*(2), 279–291, doi:10.1175/1520-0493(1997)125<0279:AWADCO>2.0.CO;2.
Oliveira, F. N. M., L. M. V. Carvalho, and T. Ambrizzi (2014), A new climatology for Southern Hemisphere blockings in the winter and the combined effect of ENSO and SAM phases, *Int. J. Climatol.*, *34*(5), 1676–1692, doi:10.1002/joc.3795.
Oliver, E. C. J., and K. R. Thompson (2011), A reconstruction of Madden–Julian Oscillation variability from 1905 to 2008, *J. Clim.*, *25*(6), 1996–2019, doi:10.1175/JCLI-D-11-00154.1.
Oliver, E. J. (2014), Multidecadal variations in the modulation of Alaska wintertime air temperature by the Madden–Julian Oscillation, *Theor. Appl. Climatol.*, doi:10.1007/s00704-014-1215-y.
Prohaska, F. (1976), *The Climate of Argentina, Paraguay, and Uruguay*, vol. 12, edited by W. Schwerdtfeger, Elsevier, Amsterdam, Netherlands.
Rasmussen, L. A., H. Conway, and C. F. Raymond (2007), Influence of upper air conditions on the Patagonia icefields, *Global Planet. Change*, *59*(1–4), 203–216, doi:10.1016/j.gloplacha.2006.11.025.

Salby, M. L., and H. H. Hendon (1994), Intraseasonal behavior of clouds, temperature, and motion in the tropics, *J. Atmos. Sci.*, *51*(15), 2207–2224, doi:10.1175/1520-0469(1994)051<2207:IBOCTA>2.0.CO;2.

Seo, K.-H., W. Wang, J. Gottschalck, Q. Zhang, J.-K. E. Schemm, W. R. Higgins, and A. Kumar (2009), Evaluation of MJO forecast skill from several statistical and dynamical forecast models, *J. Clim.*, *22*(9), 2372–2388, doi:10.1175/2008JCLI2421.1.

Sperber, K. R. (2003), Propagation and the vertical structure of the Madden–Julian Oscillation, *Mon. Weather Rev.*, *131*(12), 3018–3037, doi:10.1175/1520-0493(2003)131<3018:PATVSO>2.0.CO;2.

Vecchi, G. A., and N. A. Bond (2004), The Madden-Julian Oscillation (MJO) and northern high latitude wintertime surface air temperatures, *Geophys. Res. Lett.*, *31*, L04104, doi:10.1029/2003GL018645.

Wheeler, M. C., and H. H. Hendon (2004), An all-season real-time multivariate MJO index: Development of an index for monitoring and prediction, *Mon. Weather Rev.*, *132*(8), 1917–1932, doi:10.1175/1520-0493(2004)132<1917:AARMMI>2.0.CO;2.

Willis, M. J., A. K. Melkonian, M. E. Pritchard, and J. M. Ramage (2012), Ice loss rates at the Northern Patagonian Icefield derived using a decade of satellite remote sensing, *Remote Sens. Environ.*, *117*(0), 184–198, doi:10.1016/j.rse.2011.09.017.

Yoo, C., S. Feldstein, and S. Lee (2011), The impact of the Madden-Julian Oscillation trend on the Arctic amplification of surface air temperature during the 1979–2008 boreal winter, *Geophys. Res. Lett.*, *38*, L24804, doi:10.1029/2011GL049881.

Zhang, C. (2005), Madden-Julian Oscillation, *Rev. Geophys.*, *43*, RG2003, doi:10.1029/2004RG000158.

Zhang, C. (2013), Madden–Julian Oscillation: Bridging weather and climate, *Bull. Am. Meteorol. Soc.*, *94*(12), 1849–1870, doi:10.1175/BAMS-D-12-00026.1.

Zhou, Y., K. R. Thompson, and Y. Lu (2011), Mapping the relationship between Northern Hemisphere winter surface air temperature and the Madden–Julian Oscillation, *Mon. Weather Rev.*, *139*(8), 2439–2454, doi:10.1175/2011MWR3587.1.